Autoionizing resonances in electron-impact ionization of O^{5+} ions

A. Müller,[1] H. Teng,[1] G. Hofmann,[1] R. A. Phaneuf,[2] and E. Salzborn[1]
[1]*Institut für Kernphysik, Justus-Liebig-Universität Giessen, D-35392 Giessen, Germany*
[2]*Department of Physics, University of Nevada, Reno, Nevada 89557*
(Received 28 April 2000; published 15 November 2000)

We report on a detailed experimental and theoretical study of electron-impact ionization of O^{5+} ions. A high-resolution scan measurement of the *K*-shell excitation threshold region has been performed with statistical uncertainties as low as 0.03%. At this level of precision a wealth of features in the cross section arising from indirect ionization processes becomes visible, and even interference of direct ionization with resonant-excitation/auto-double-ionization (READI) is clearly observed. The experimental results are compared with *R*-matrix calculations that include both direct and indirect processes in a unified way. Radiative damping of autoionizing Li-like states is found to be about 10–15 %. The calculations almost perfectly reproduce most of the experimental resonance features found in the present measurement including READI. They also agree with the direct-ionization converged close-coupling results of I. Bray [J. Phys. B **28**, L247 (1995)] and the absolute total ionization cross section measurement of K. Rinn *et al.* [Phys. Rev. A **36**, 595 (1987)].

PACS number(s): 34.80.Dp, 34.80.Kw

I. INTRODUCTION

Atomic data needs for ionization cross sections and rate coefficients relevant to laboratory and astrophysical plasmas have stimulated extensive theoretical and experimental efforts to investigate and understand the direct and indirect ionization mechanisms in electron-impact ionization of atomic ions [1,2]. Experimental techniques have been developed to observe fine detail in ionization cross sections and to study especially the physics of indirect ionization mechanisms. High-quality results for autoionizing resonances have been obtained, particularly in measurements with ions of the lithium and sodium isoelectronic sequences [3–10]. Theoretical attempts to describe the dominant features in the measured ionization cross sections by the independent-process approximation were quite successful. Stimulated by the experimental results and also by the interest in quasi-one-electron systems, detailed calculations have also concentrated on the lithium and sodium isoelectronic sequences. Most of this work has been reviewed by Moores and Reed [2]; some of the later results have been described in combination with subsequent experimental work (see, e.g., [7–9]). So far, theory has suffered from being unable to treat all relevant indirect processes in a unified way. It was not until recently that this problem was partly solved by Berrington *et al.* [11] using a unified *R*-matrix method and by Scott *et al.* [12] using a unified RMPS (*R* matrix with pseudostates) method in which both direct and indirect ionization mechanisms as well as interference between them are consistently included. Variations of this method have been applied to several ions in low charge states already: Be^{+} [11], C^{3+} [13], Mg^{+} [14], Al^{2+} [15], and Li^{+} [16,17]. Whenever comparisons with experiments could be made, a high degree of agreement was found.

In this paper we report detailed experimental and theoretical results for electron-impact ionization of O^{5+} ions. Within the sequence of theoretical studies using the unified *R*-matrix approach this is the highest charge state of all ions investigated so far. Unlike previous calculations, effects of radiative damping have to be considered in this case. Special attention was directed to resonance features in the energy range just below and above the *K*-shell excitation threshold. Autoionizing resonances were measured with high precision and high energy resolution and calculated using the unified *R*-matrix method. Many of the dominant features seen in this work had already been observed previously, although with less precision in the experiment [4] and with certain deficiencies in the theoretical description [18–20]. In particular, no satisfactory theoretical treatment had been available for resonance contributions proceeding via radiationless capture of the projectile electron by the target ion and subsequent simultaneous emission of two target electrons in a double Auger process. It has been shown previously that this process, termed resonant-excitation/auto-double-ionization (READI) [see Eq. (4) below] contributes to the cross section for net single ionization of ions by electron impact [3,4].

By improving the experimental precision in the present work, a number of additional features could be detected and fresh observations made. In particular, with the present experimental and theoretical study we are able to establish the presence of interference between direct ionization and complex resonant multielectron interaction channels (such as READI) visible in the total single-ionization cross section of O^{5+} ions.

For electron-impact ionization of O^{5+}, in addition to the direct ionization (DI)

$$e^{-}+O^{5+}(1s^{2}2s)\rightarrow\begin{cases}O^{6+}(1s^{2})+2e^{-}\\ O^{6+}(1s2s)+2e^{-}\end{cases}\qquad(1)$$

of either a *K*-shell or *L*-shell electron, three important indirect processes can contribute to the total ionization cross section. These are nonresonant excitation/autoionization (EA)

$$e^- + O^{5+}(1s^2 2s) \rightarrow O^{5+*}(1s2snl) + e^- \quad \text{(2)}$$
$$\hookrightarrow O^{6+}(1s^2) + e^-,$$

resonant-excitation/double-autoionization (REDA)

$$e^- + O^{5+}(1s^2 2s) \rightarrow O^{4+*}(1s2snln'l') \quad \text{(3)}$$
$$\hookrightarrow O^{5+*}(1s2sn''l'') + e^-$$
$$\hookrightarrow O^{6+}(1s^2) + e^-,$$

and resonant-excitation/auto-double-ionization

$$e^- + O^{5+}(1s^2 2s) \rightarrow O^{4+*}(1s2snln'l') \quad \text{(4)}$$
$$\hookrightarrow O^{6+}(1s^2) + 2e^-.$$

The resonant ionization channels involve dielectronic capture of the incident electron in a first step which is then followed by the emission of two electrons from the intermediate highly excited state. This emission happens in two separate steps in the case of the REDA mechanism [Eq. (3)] and in one single event, a double Auger process, in the case of the READI process [Eq. (4)]. Apart from the inherent complexity of such multistep correlated processes involving interactions of several electrons at a time, an additional complication is introduced by the fact that different ionization channels may be open at a given energy and cannot be distinguished experimentally. This can lead to interference effects whose theoretical description requires a unified treatment of all possible reaction channels.

An overview of the energetics of electron-impact ionization of O^{5+} ions is provided in Fig. 1. In addition to the energy levels of the lithiumlike ion target, those of the heliumlike (ionized) target system, and resonances in the berylliumlike (recombined) target system are also relevant. Samples for the reaction pathways described by Eqs. (1) through (4) are shown by arrows in the figure, which contains all energy levels of the lithiumlike states that were included in the present *R*-matrix theory plus several additional levels in the Be-like and He-like system that were explicitly determined and identified on the basis of the *R*-matrix wave function constructed in this work. Figure 1 also shows the energies of pseudostates used in the present calculation. For more details, see Sec. III of this paper.

Experimental work on O^{5+} started with a cross section measurement by Crandall *et al.* in 1979 [21], which already showed the presence of EA in the total net single-ionization cross section but had quite big uncertainties due to the difficulty of producing sufficiently high currents of O^{5+} ions at that time. Crandall *et al.* repeated the experiment later [22] when a newly installed electron-cyclotron-resonance (ECR) ion source became available at Oak Ridge National Laboratory (ORNL). The data set of [22] is shown by the open squares in Fig. 2. An apparent excursion of the cross section at electron energies above 400 eV was interpreted as a possible consequence of contributions of the READI mechanism

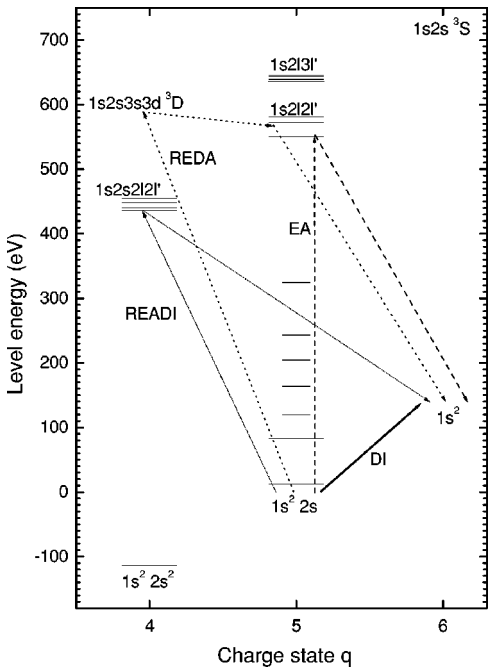

FIG. 1. Energy level diagram with some of the states relevant to the ionization of O^{5+} ions. Direct ionization (DI, solid arrow) leads from the $1s^2 2s\ ^2S$ ground state of O^{5+} $(q=5)$ to the $1s^2\ ^1S$ ground state of O^{6+} $(q=6)$. Excitation/autoionization (EA, long-dashed arrow lines) populates multiply excited states with configurations $1s2snl$ of the O^{5+} ion, which then decay to the ground state of O^{6+}. Resonant-excitation/double-autoionization (REDA, short-dashed arrow lines) populates multiply excited resonant states of O^{4+} $(q=4)$ with configurations $1s2snln'l'$, which can decay in two steps via an intermediate doubly excited state of O^{5+} finally into the ground state of O^{6+}. Resonant-excitation/auto-double-ionization (READI, dotted arrow lines) also populates multiply excited resonant states of O^{4+} $(q=4)$ with configurations $1s2snln'l'$, which then decay in one single step into the ground state of O^{6+}. Energies were calculated within the framework of *R*-matrix calculations. In particular, all basis states of the present *R*-matrix calculations are indicated. The five pseudostates are identified by the short level bars. For more details see Sec. III.

[cf. Eq. (4)]. This in turn stimulated the subsequent measurements of Rinn *et al.* [23], who were able to reduce the relative uncertainties of closely spaced data points (step width approximately 1.2 eV) to the level of 0.4% by using the well established ORNL crossed-beam arrangement. Around the expected READI resonances the density of points was even enhanced to about 3 per eV. However, the energy scan measurement did not provide real evidence for the observation of READI.

A year later, Müller *et al.* introduced an energy scanning technique to their experiments using a high-current electron gun, which allowed them to identify REDA and also READI mechanisms in a number of ions [3,24]. Hofmann *et al.* [4] carried out a scan measurement of the electron-impact single ionization of O^{5+} ions using an energy step width of less than 0.04 eV. By combining packets of five of these data points, effectively going to 0.2 eV step width, Hofmann *et al.* reduced their statistical uncertainties to the level of 0.1% and by that found clear evidence for the presence of

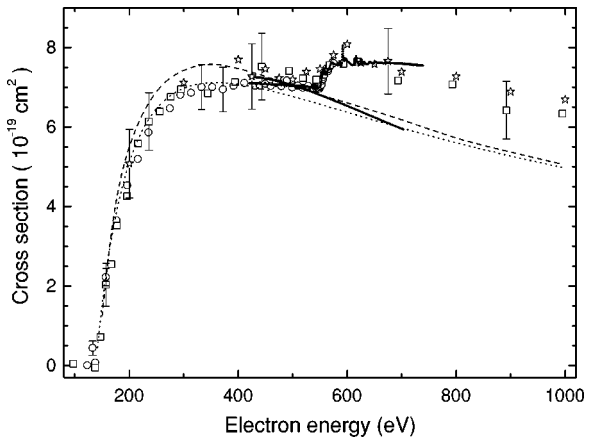

FIG. 2. Overview of ionization cross sections for O^{5+}. Previous experimental data of Crandall *et al.* [22] are shown by open squares. The asterisks are separate absolute cross section data from the previous measurement series of Hofmann *et al.* [4]. For the present display, the latter were multiplied by a constant factor of 0.77. The present experimental scan data are shown by small solid dots (not resolved in the present reduced figure size). They were normalized to the absolute measurement of Rinn *et al.* [23] which is represented by the open circles. The error bars displayed in the figure are representative for the absolute quoted uncertainties of the different experiments. Theoretical results for the DI contribution [excluding all indirect ionization mechanisms; see Eq. (1)] are displayed by lines: present *R*-matrix calculation of DI only (solid line), Bray's CCC (converged close-coupling) calculation [27] (dashed line), Younger's DWE (distorted-wave with exchange) calculation [28] (dotted line).

READI and numerous REDA and EA features in the ionization of O^{5+}. The scan measurement of Hofmann *et al.* was complemented by a separate absolute measurement of the total single-ionization cross section which served as a normalization of the relative scan measurement. The cross sections obtained in that experiment were close to 1×10^{-18} cm^2 at the cross section maximum and thus differ from the ORNL data by an amount slightly beyond the sum of the total absolute error bars of the two experiments. The reason for this discrepancy is presently not understood and merits further attention.

On the theory side, an attempt to calculate resonant contributions to the ionization of Li-like ions was made by Pindzola and Griffin [18], who estimated the resonance strength $S=\int \sigma_{READI}(E)dE$ of a single READI resonance with cross section $\sigma_{READI}(E)$. The selected resonance was associated with the intermediate $1s2s^22p\,^3P$ Be-like *K*-shell-excited state. The upper and lower limits provided for *S* by that theoretical approach were 9.8×10^{-21} cm^2 eV and 1.2×10^{-21} cm^2 eV, respectively, i.e., the uncertainty of σ at the peak of the $1s2s^22p\,^3P$ resonance was more than a factor 8. This large uncertainty factor reflects the great difficulty of determining decay rates for processes with three directly interacting electrons and simultaneous emission of two of them. Such simultaneous two-electron emission, or double Auger decay, is the only mechanism by which a resonantly excited $1s2s^22p\,^3P$ Be-like state can end up as $1s^2$ He-like and thus contribute to the ionization channel.

The 17-state *R*-matrix close-coupling calculation of Tayal and Henry [19] produced detailed results on indirect ionization of O^{5+} ions. The processes described by Eqs. (2) and (3) were included in the calculation. However, Tayal and Henry were unable to deal with the more complex mechanism, READI, represented by Eq. (4). In their calculation the total ionization cross section was obtained by adding their calculated contributions of indirect processes to distorted-wave results for direct ionization. Interference between direct and indirect processes was thus neglected. Reed and Chen [20] calculated the total ionization cross section in an independent-process relativistic distorted-wave approximation where DI, EA, and REDA [cf. Eqs. (1)–(3)] were considered to be independent. READI could also not be treated by these authors either. Nevertheless, overall the *R*-matrix and relativistic distorted-wave calculations were in quite good agreement with the EA and REDA features observed in the experiments of Hofmann *et al.* [4].

While the above calculations concentrated on the indirect ionization mechanisms and understanding of the numerous cross section features found in the scan experiment, a theoretical attempt is presently being made to understand direct ionization better and to produce reliable cross sections for DI of a wide range of ions in different charge states. Recent work on this topic has been published by Badnell *et al.* [25], Mitnik *et al.* [26], and Scott *et al.* [12]. Among the recent theoretical efforts only a converged close-coupling (CCC) calculation of Bray [27] is available for DI of O^{5+} ions. As Fig. 2 shows, the CCC calculation is in quite good agreement with the previous distorted-wave exchange (DWE) result of Younger [28]. Both theoretical cross sections agree well with the experimental DI data of Crandall *et al.* [22] and Rinn *et al.* [23], i.e., with measured cross sections below the EA threshold at 550 eV.

A complete calculation including DI, EA, REDA, and READI processes for electron-impact single ionization of O^{5+} did not exist prior to the present work to our knowledge. In the present study, experiments considerably improved with respect to our previous work are accompanied by a unified *R*-matrix calculation for O^{5+} ions in the energy range below and above the EA threshold, where resonances associated with the processes described by Eqs. (3) and (4) can occur.

II. EXPERIMENT

The experiment was carried out using the crossed-beam setup described by Tinschert *et al.* [29] augmented with a 10 GHz ECR ion source [30]. Experimental techniques and procedures have been discussed in some detail previously by Müller *et al.* [31] and again by Hofmann *et al.* [4]. Therefore the description of the present measurements can be kept comparatively short.

A collimated 50 keV O^{5+} ion beam of typically 4 mm diameter with an electrical current of up to 3 μA was crossed with an intense ribbon shaped electron beam extending 6 cm in the ion beam direction. The height of the electron beam (the ribbon thickness) somewhat depends on the electron energy and in the range of the present measurements it

is of the order of 2.5 mm [32]. The electron beam can be mechanically moved out of the way of the ion beam during a measurement, which allows for the determination of both beam overlap factors and detector background. Electron currents are as high as 125 mA at 420 eV and 290 mA at 730 eV, corresponding to densities 4.3×10^{8} cm^{-3} and 7.6×10^{8} cm^{-3}, respectively. Thus, counting rates of ionized O^{6+} ions of the order of 100 to 500 kHz were available.

The detector for the ionized ions was of the type described previously by Rinn *et al.* [33]. It has a detection efficiency of $(97\pm3)\%$ for ions in the energy range of tens of keV. The fast channel electron multiplier used in this detector had a dark count rate of only about 0.1 s^{-1}. The detector together with the subsequent electronic devices had a dead time of about 0.4 μs resulting in efficiency losses of up to 20% at the highest counting rates. Absolute measurements of cross sections are therefore restricted to maximum counting rates of 30 to 50 kHz, which can always be accomplished by reducing the ion current. For relative cross section measurements partial loss of signal can be tolerated as long as the variations in the counting rates are small within one sequence of cross section measurements. Typical detector background (with the electron beam switched off or, alternatively, with no overlap of the electron and ion beams) was below 20 kHz. The electron beam itself did not produce detector counts, nor did the ion collection in a Faraday cup located inside the vacuum chamber of the analyzing magnet. The background was determined only by stripping of the parent ions in the residual gas of the interaction chamber.

The base pressure in the collision chamber was less than 10^{-9} mbar; however, Kr gas was introduced into the interaction region with a pressure of typically 10^{-7} mbar in order to offset the space charge of the electron beam by slow ions produced by the electron beam interacting with the gas. Even with the Kr gas present in the interaction region, detector backgrounds (see the numbers given above) were almost negligible since the stripping cross sections for multiply charged ions at low velocities are small. In the present case the ion velocity was only about one-tenth of the average orbital velocity of the outermost electron in the O^{5+} ion. Under such conditions stripping of this electron is an unlikely process.

The space charge potential depression in an infinitely wide (ribbon shaped) electron beam of particle density n_e and height h is

$$\Delta U = h^2 e n_e / 8\varepsilon_0, \tag{5}$$

where e is the charge of an electron and ε_0 is the permittivity of vacuum. Inserting into Eq. (5) the numbers given above for an electron energy of 730 eV results in a potential difference between the center plane and the surface of the electron beam of $\Delta U = 10.7$ V. The resulting space charge fields can lead to a (slight) deflection of the ion beam and, worse, ΔU directly determines the energy resolution possible with such an electron beam.

In the present geometry, trajectory and field calculations that include the effects of electron space charge show the presence of a potential distribution that is able to trap positive ions. The trap depth, i.e., the voltage between the central plane of the electron beam and the grounded electrode surrounding the beam, is as much as 4% of the cathode voltage, i.e., 29.2 V at 730 V. Our measurements indicate that this trap is almost completely filled and already compensated by positive ions at the low base pressure. With gas introduced to the collision region cross section features shift in energy by only a few eV (instead of possibly 29.2 eV in the example given above). The energy resolution is almost uninfluenced by the pressure in the interaction region, indicating that the ion beam probes a region of the electron beam that has a rather flat (already partially compensated) space charge potential distribution at all accessible background gas pressures.

At pressures beyond about 1×10^{-7} mbar cross sections and resonance positions do not change any more, indicating saturation of space charge compensation. This saturation involves a substantial target of slow krypton ions for the ion beam in addition to the electron beam. By measurements of apparent electron-impact ionization cross sections with the electron energy reduced to values below the ionization threshold one can test the possible effect of the ion target [31]. In almost all our ionization experiments negligible signal rates, potentially originating from ion-ion collisions within the electron beam, were observed below the ionization threshold of the parent ions. Also, collisions of fast O^{5+} with slow trapped Kr ions would not produce any sharp cross section features (dielectronic capture resonances and abrupt excitation steps) when the electron energy is changed. They would rather produce a smooth background in the total cross section.

For the observation of fine detail, the ionization cross section was measured in the energy range 420 to 740 eV using the energy scanning technique introduced by Müller *et al.* [24]. With optimized overlap of the intersecting beams the electron energy was ramped over preset ranges of typically 40 eV in 1024 steps of 0.039 eV each and a dwell time of only about 3 ms at each energy. The number of counts collected on the O^{6+} detector during the electronically gated dwell time on each given electron energy was recorded together with the related electron and ion beam currents I_e and I_i, respectively, averaged over the identical gate time intervals. The true gate time for each energy was also measured and recorded. Including the voltage-set and scaler-read-out time intervals of 0.3 ms, one complete energy scan took little over 3 s. The scans were automatically repeated until the counting statistics had reached a desired level.

The background measured with the electron beam displaced such that there was no overlap with the ion beam was measured in the same fashion. This background depends only very slightly on the electron energy because of increasing outgassing of surfaces in the collision region as the electron beam power increases. After subtraction of the background, the energy dependent true signal rate R is obtained, from which the cross section can be calculated:

$$\sigma(E) = \frac{R}{I_e I_i} \frac{q e^2 v_i v_e}{(v_e^2 + v_i^2)^{1/2}} F. \tag{6}$$

Here, q $(=5)$ is the charge state of the parent (O^{5+}) ion, e is the electron charge, v_i and v_e are the velocities of ions and electrons, respectively, E is the center-of-mass energy in the electron-ion system, and F is the form factor describing the overlap of the two beams. This form factor cannot be measured explicitly for each energy during a scan measurement. Comparisons of absolute cross sections obtained in measurements following the technique of Müller *et al.* [31] with cross section energy dependences measured by the scanning technique show that in the case of optimum overlap the form factor can be approximated over a wide energy range by

$$F \approx h \approx \{-0.44 + 1.39 \log_{10}[E\ (\mathrm{eV})]\}^{-1}\ \mathrm{cm}. \qquad (7)$$

With this approximation a relative cross section $\sigma(E)$ was determined for each energy scan by inserting $F(E)$ from Eq. (7) into Eq. (6). Numerous individual overlapping energy scans were then combined. For this purpose an arbitrary scan was selected forming the nucleus of a ''master data set.'' Then the neighboring scans were multiplied by constant factors such as to bring the cross sections into relative agreement with the master set in the overlap region. Subsequently the scans were added with the overlapping cross sections averaged. By repeating the procedure with the growing scan-data master set the final relative scan measurement was obtained. Since the resulting data sets are not normalized to an absolute scale, separate absolute cross section measurements are necessary to provide the scale for the scan data. Since the present measurement was focused on the detection of cross section details that had not been accessible previously, a separate absolute measurement was deferred.

As mentioned above, the previous absolute measurement by Hofmann *et al.* [4] that served for the normalization of the associated scan data is higher than the different data sets obtained at ORNL. The reason for this discrepancy is presently not known. Further experiments will be necessary to clarify the existing differences between different experimental setups and techniques. For the present study we chose to normalize our scan data to the absolute cross sections measured by Rinn *et al.* [23] at ORNL. The normalization involved a constant factor (of 1.2 in the present case) for the whole spectrum. This factor was determined by comparing the heights of the EA step at 550–580 eV in the relative scan and the absolute measurement. In addition, it was necessary to subtract a straight line from the energy dependent scan cross section to match the energy dependence of the data of Rinn *et al.* As Fig. 2 reveals, the cross section of Rinn *et al.* shows an unusually flat energy dependence below the EA threshold. All other data sets, including the theoretical results, suggest a decreasing DI cross section at energies above about 400 eV. The differences are relatively small on the scale of the absolute total cross section and are included in the total error bars of the different experiments. On the scale of the indirect contributions to the ionization cross section, however, these small differences become rather big and would make a detailed comparison of theory with experiment difficult. Therefore, in the context of the fine detail of the ionization cross section the comparisons in this paper are made after subtracting the smooth DI contribution so that the resonance and step features arising from indirect ionization mechanisms become more easily visible.

The measurement of Rinn *et al.* [23] has a quoted total relative uncertainty at the peak of the cross section of $\pm 8\%$ at the 90% confidence level. Consequently, this is also the uncertainty of the present overall cross section function. Relative uncertainties of the indirect cross section contributions are considerably higher because of the possible error in determining the true DI contribution and due to the fact that there is also uncertainty in the energy dependent form factor described by Eq. (7). The related error bars are of the order of up to 30%. However, the relative sizes of closely spaced cross section features have very small uncertainties. In fact, relative errors in resonance strengths of REDA peaks adjacent to each other can be assumed to be less than 1%. This strong statement can be made on the basis of the low relative uncertainties of the present point-to-point measurements with their excellent statistics and the fact that all normalization functions like the form factor $F(E)$ are very slowly varying with the electron energy compared to the energetically narrow features observed in the present experiment.

As in the previous work of Hofmann *et al.* packets of five data points were combined to get one cross section with improved statistics. Still, the resulting data points cover an energy range from 420 eV to 740 eV in more than 1600 steps. In this context it may be interesting to note that some 10^{10} O^{6+} product ions were counted in the present experiment. The data analysis shows that the energy spread in the experiment was close to $\Delta E = 2.5$ eV in the energy range investigated, i.e., the energy resolution at $E = 600$ eV amounts to $E/\Delta E \approx 240$ without the use of an energy filter for the electron beam. The uncertainty of the energy calibration depends on the degree of electron space charge compensation by slow residual gas ions. In a detailed analysis Hofmann *et al.* [4] have shown that level energies inferred from our scan measurements are almost always within ± 1 eV of spectroscopic data in the literature. This general observation is again supported by the present measurement.

Under the experimental conditions briefly outlined above, the counting statistics of the present results could be considerably improved over the previous measurement of Hofmann *et al.* [4]. By reducing relative uncertainties of the cross section scan in the range of the dominant READI features (420–460 eV) to less than 1/3, i.e., 0.03%, while keeping the energy density of data points the same, additional unexpected features in the cross section became visible, and other features that had already been observed previously have now become more clear and allow for an interpretation without ambiguity. In general, the structures observed in the experiment of Hofmann *et al.* are perfectly well reproduced, supporting the confidence we have in the relative precision of our scan measurements. The additional features detected by the present experiment with its much increased quality will be discussed in more detail below.

III. THEORY

A complete theoretical description of both direct and indirect ionization processes demands a unified total wave

function. The *R*-matrix method uses a close-coupling approach, in which the total $(N+1)$-electron wave function is expanded in terms of an *N*-electron target basis, which contains the required initial and final states and other states that are strongly coupled to these. However, such an expansion over target bound states is not complete if the probability of ionization is significant. In that case, the calculation should include an integral over the continuum, represented by a product of the final state wave function of the *N*-electron system and the electron scattering function.

A convenient way of representing this integral while retaining the simplicity of the close-coupling expansion is to use a pseudostate discretization to approximate the integration [34]. Such an approach has been shown to give good convergence over a wide range of energies (see, e.g., [26]), but can involve large sets of pseudostates; at present it would be computationally difficult to include inner-shell autoionizing states also in these expansions. However, Berrington *et al.* [11] suggested that at a given (high) energy *E* the open channel part of the integral, which is continuous in the energy range below *E*, can be formally approximated by a mean value in the range. They therefore examined the possibility of introducing energetically allowed pseudostates $\overline{nl}$ for each target angular momentum *l* to approximate the direct cross section into the continuum, and found for Be^+ and Li^+ that suitable pseudostates could be constructed from orbitals optimized on the inner-shell states. Thus, the total ionization cross section becomes a sum of partial cross sections for excitation to all Li-like basis states embedded in the first ionization continuum (see Fig. 3):

$$\sigma_{\text{ionization}}(E) \approx \sum_{nl} \sigma_{\overline{nl}} + \sigma_{\text{autoionization}}. \tag{8}$$

This approximation is energy dependent. However, in a region where the direct ionization cross section varies only slowly with energy, the approximation can be expected to be good over a reasonable range of energies. Berrington *et al.* [11], however, found that the ionization cross section was likely to be overestimated in this approach unless a further pseudostate, optimized on the dipole polarizability of the ground state, was included in the bound state spectrum to allow for loss of flux into the infinity of dipole-coupled bound states.

In a recent publication, Scott *et al.* applied this theoretical technique to the electron-impact ionization of C^{3+} ions and found very good agreement with the results of the most advanced theoretical representations of DI [12,26] and with the detailed results of a recent cross section measurement [13]. In the present work as well as in the calculation for C^{3+} ions, we adopted the procedure that is briefly outlined above. Unlike the work of Berrington *et al.* [11], the present calculations additionally comprise a real $3p$ orbital and a $\overline{5p}$ polarized orbital for better representation of the total unified wave function. This allows us to obtain valid theoretical results for an extended energy range.

As mentioned above, the unified *R*-matrix method describes both direct and indirect ionization processes with a unified total wave function constructed with a set of common

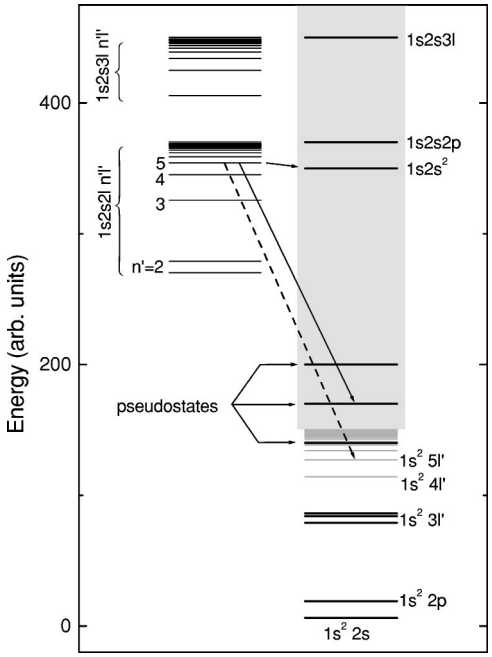

FIG. 3. Schematic energy level diagram for a (3+1)-electron system as treated by the present *R*-matrix approach. Singly excited bound levels of a Li-like ion are indicated above the $1s^2 2s$ ground state extending up to the ionization threshold. The continuum above that threshold is represented by the shaded area. Embedded in the continuum, a few doubly excited states are indicated. Although the *R*-matrix calculation comprises many more physical states (see Fig. 1), including the complete (infinite) Rydberg series of Be-like levels attached to each of those Li-like states, the present basis set is restricted in that all Li-like states with principal quantum numbers $n' \geqslant 4$ are excluded. The missing states are indicated by the light horizontal bars. They are represented by introducing pseudostates situated below the ionization threshold. The continuum above this threshold is represented by a number of other pseudostates. Resonant contributions to ionization are represented by their contributions to excitation of these unbound pseudostates (READI) and the doubly excited autoionizing states (REDA). Examples of such channels are indicated by the two solid arrows starting from an intermediate $1s2s2l5l'$ level. The loss of ionization strength by single Auger transitions to a bound $1s^2 5l'$ state is indicated by the dashed arrow.

orbitals. The real target states and the pseudostates are defined on the basis of these orbitals. For O^{5+} ions, we used five physical bound states $1s^2 2s\,^2S$, $1s^2 2p\,^2P$, $1s^2 3s\,^2S$, $1s^2 3p\,^2P$, and $1s^2 3d\,^2D$, five pseudostates of the type $1s^2\overline{4s}\,^2S$, $1s^2\overline{4p}\,^2P$, $1s^2\overline{4d}\,^2D$, $1s^2\overline{4f}\,^2F$, and $1s^2\overline{5p}\,^2P$, as well as 16 $1s2l2l'$, $1s2s3l'$ autoionizing states, i.e., a total of 26 spectroscopic states and pseudostates. The energies calculated for these states are shown in Fig. 1 and listed in Table I. They are in excellent agreement with other calculations and with the available experimental data.

The target states and pseudostates are then included in the *R*-matrix calculation to represent the DI, EA, REDA, and READI channels. Since the *R*-matrix method is a close-coupling technique, the possibility for interference between direct and indirect processes as well as between different

TABLE I. Energies of the 26 lowest states and pseudostates of O^{5+} included in the *R*-matrix calculation. The ionization potential of O^{5+} is 138.116 eV. E_i, present calculation; E_{TH}, calculation of Tayal and Henry [19]; E_{NIST}, experimental data taken from the NIST Atomic Database [39]; E_{RBB}, experiment of Rødbro *et al.* [43].

States	E_i	E_{TH}	E_{NIST}	E_{RBB}
$1s^2 2s\ ^2S^e$	0.0	0.0	0.0	0.0
$1s^2 2p\ ^2P^o$	11.95		11.99	
$1s^2 3s\ ^2S^e$	79.26		79.35	
$1s^2 3p\ ^2P^o$	82.50		82.60	
$1s^2 3d\ ^2D^e$	83.51		83.65	
$1s^2\overline{4p}\ ^2P^o$	119.60			
$1s^2\overline{4d}\ ^2D^e$	163.93			
$1s^2\overline{4s}\ ^2S^e$	204.19			
$1s^2\overline{4f}\ ^2F^o$	243.23			
$1s^2\overline{5p}\ ^2P^o$	324.67			
$1s2s^2\ ^2S^e$	550.44	551.45		550.7
$1s2s(^3S)2p\ ^4P^o$	553.60	555.23	554.24	554.1
$1s2s(^1S)2p\ ^2P^o$	563.26	563.30	563.04[a]	563.1
$1s2p^2\ ^4P^e$	566.73	567.81[b]	567.2	
$1s2s(^3S)2p\ ^2P^o$	567.58	569.07	567.56[a]	568.1
$1s2p^2\ ^2D^e$	572.25	573.70	572.49	
$1s2p^2\ ^2P^e$	574.57	574.29	574.43	
$1s2p^2\ ^2S^e$	581.14	582.62	581.22	
$1s2s(^3S)3s\ ^4S^e$	635.58	637.19	635.90	
$1s2s(^3S)3s\ ^2S^e$	638.37	639.36		
$1s2s(^3S)3p\ ^4P^o$	639.46	640.76		
$1s2s(^3S)3p\ ^2P^o$	639.92	642.36		
$1s2s(^3S)3d\ ^2D^e$	643.57			
$1s2s(^1S)3s\ ^2S^e$	644.90			
$1s2s(^1S)3p\ ^2P^o$	646.98			
$1s2s(^1S)3d\ ^2D^e$	650.28			

[a]We suppose there are misidentifications for the $1s2s(^1)2p\ ^2P^o$ and $1s2s(^3S)2p\ ^2P^o$ states in the table of NIST Atomic Spectra Database for O^{5+}. The lower energy level should be $1s2s(^1S)2p\ ^2P^o$ rather than $1s2s(^3S)2p\ ^2P^o$.

[b]The number given in the paper (Ref. [19]) is 676.81 eV, which we consider to be a misprint.

indirect ionization channels is automatically incorporated in all orders.

All target states and pseudostates were represented by configuration interaction wave functions. Eleven orbitals were used. The $1s$, $2s$, $2p$, $3s$, $3p$, and $3d$ orbitals were taken from the table given by Weiss [35]; these orbitals give good excited state wave functions. The $\overline{4s}$, $\overline{4p}$, $\overline{4d}$, and $\overline{4f}$ orbitals were optimized on the $1s2s^2$, $1s2p^2$, and $1s2s2p$ inner-shell excited states, using the CIV3 package of Hibbert [36]; and the $\overline{5p}$ polarized orbital was optimized on the $1s^2 2s$ ground state dipole polarizability. The target orbitals require an *R*-matrix radius of 8.0 a.u. and 26 continuum basis functions were used per angular momentum. The internal region *R*-matrix package RMATRX II [37] and the external asymptotic program STGF [38] were employed. Partial waves up to total angular momentum $L=20$ were needed to obtain converged results for the ionization cross sections. A top-up procedure was used to check for possible contributions of higher partial waves and they were found to be negligible. Finally, the total cross section for ionization from the ground state was calculated by summing the excitation cross sections for transitions into all the autoionizing states and pseudostates lying above the ionization threshold of the ground state, i.e., 138.119 eV [39].

It should be pointed out that the result of this summation partly overestimates the ionization cross section because there are two loss mechanisms that cannot be directly accounted for in the *R*-matrix calculation described above. The first is radiation damping, which can reduce the contribution of the EA, REDA, and READI processes to the total ionization cross section by radiative decay; and this effect increases with the ion charge state. In the present work, the effect of radiation damping on the EA process has been treated by separately determining the branching ratios for autoionization and radiative decay of all doubly excited Li-like states included in our *R*-matrix calculation, using the same wave functions and orbitals. The effect of radiation damping on the resonant (REDA and READI) contributions could not be determined in the framework of the present unified *R*-matrix theory. However, the work of Reed and Chen [20] has shown that radiative corrections are of the order of only 1% for the REDA resonances on the O^{5+} core and one can assume that this is also true for the READI resonances.

The second loss mechanism that cannot be directly accounted for in the present *R*-matrix calculations is the effect of flux loss into infinite Rydberg series of states with Li-like configuration $(1s^2 nl)$. This can be described as follows: intermediate (O^{4+}) resonant states with configurations $1s2snln'l'$ produced by dielectronic capture of the incident electron can eventually decay (i) by two sequential autoionization processes and thus contribute to single ionization via the REDA channel, or (ii) by simultaneous emission of two electrons and thus contribute to single ionization via the READI channel. However, these same states can also decay to a bound Li-like configuration via a single Auger process

$$e+1s^2 2s \rightarrow 1s2snln'l' \rightarrow 1s^2 n'l'+e. \tag{9}$$

In this case the resonant population of those intermediate states does not contribute to ionization and hence potential ionization strength is lost. The alternative decay routes in the present *R*-matrix picture are indicated in Fig. 3 for one particular intermediate resonant level with configuration $1s2s2l5l'$. The upper solid arrow represents a REDA contribution, the lower solid arrow a READI contribution, and the dashed arrow the single Auger loss channel.

R-matrix calculations like the one of Tayal and Henry [19] as well as the present one are unable to account for all such loss of resonance strength because the inclusion of all the Li-like Rydberg states would necessitate an excessively large calculation, which thus defeats the purpose of the *R*-matrix method. This was pointed out by Robicheaux *et al.* [40] in a discussion concerning radiative damping. The cal-

culation of Tayal and Henry was limited by including only those $1s^2n'l'$ excited states with $n' \leqslant 3$. It therefore overestimated the resonant contribution to ionization arising from REDA processes by inherently including in the ionization channel all the pathways described by Eq. (9) for $n' \geqslant 4$, which in reality contribute to resonant inelastic scattering of the projectile electron from the ion. Reed and Chen found that this does not cause appreciable errors as long as both $n,n' \geqslant 3$. However, for $n=2$ REDA is energetically possible only if $n' \geqslant 5$, with the consequence that Tayal and Henry with their basis set limited to $n' \leqslant 3$ could not account for any losses of the type described by Eq. (9). Reed and Chen calculated the loss by using their independent-process approach and found from the branching ratios a necessary correction of the $1s2s2ln'l'$ total resonance strength by a factor of about 1/3 in order to obtain the true REDA contribution.

Unlike the previous theoretical approaches to the problem of indirect ionization of O^{5+}, the present calculation includes contributions to single ionization from all configurations $1s2s2ln'l'$ and $1s2s3ln'l'$ and it comprises both REDA and READI processes. By including all $1s2s2ln'l'$ READI resonances with $n'=2,3,\ldots,\infty$ the problem with the loss channels described by Eq. (9) becomes even more severe in the present calculation compared to previous work, where READI was totally ignored. Tayal and Henry accounted for losses to $1s^2n'l'$ states with $n'=2$ and $n'=3$ because their basis set included these most important final states of loss decays. Furthermore, they avoided all such losses for $n=2$ and $n'=2,3,4$ ''by definition,'' because they neglected READI in general. In the present calculation $n'=2$ and $n'=3$ singly excited states with configurations $1s^2n'l'$ are also included in the *R*-matrix basis set, taking care of the loss channels from $1s2s2l2l'$ and $1s2s2l3l'$ READI resonances. However, for $n' \geqslant 4$ a reduction of the calculated resonance strength is necessary to correct for losses due to processes described by Eq. (9). Again, for $n,n' \geqslant 3$ such corrections can be safely neglected.

In order to quantify the possible influence of the effects described in the previous paragraph, one has to consider all the different decay processes of the intermediate resonant states and their relative probabilities. Let us assume a $1s2s2ln'l'$ intermediate state with $n' \geqslant 4$. For a double Auger process to happen, all three excited electrons have to interact with each other, which becomes increasingly less probable as n' increases because then the spatial overlap of the electron density distributions decreases. By the same argument single Auger processes involving one *L*-shell electron and the n' Rydberg electron have low probabilities compared with those single Auger decays that involve the two *L*-shell electrons. Therefore, the dominant decay channel of $1s2s2ln'l'$ resonant states is the single Auger process involving the two *L*-shell electrons. This produces $1s^2n'l'$ final states, which cannot autoionize and thus do not contribute to net single ionization. As a consequence, the single Auger channel will increasingly dominate the double Auger decay and hence READI becomes rapidly suppressed as n' increases.

When n' is greater than or equal to 5, the $1s2s2ln'l'$ resonant state can also decay by two sequential Auger processes, thus feeding the REDA channel. However, the loss channel via single Auger decay to $1s^2n'l'$ is clearly dominant and suppresses the REDA channel to a large extent.

Bearing in mind that the READI decay involves a double Auger process, and that the much more probable single Auger channel feeds the loss mechanism, we have cut off all READI resonances from our calculated cross section in the energy range 520–570 eV, where $1s2s2ln'l'$ resonances with $n'=4,5,\ldots,\infty$ can occur. (The lowest $1s2s^24s$ state was found to be at 523 eV.) These resonances decay with a very high probability by a single Auger process, mediated by the mutual interaction of the two *L*-shell electrons, to bound $1s^2n'l'$ states. Compared to that channel the interaction of the *L*-shell electrons with the n' Rydberg electron can be expected to be negligible. Hence, the assumption of complete loss of $1s2s2ln'l'$ states with $n' \geqslant 4$ from the READI ionization channel appears to be justified.

The situation is different for those $1s2s2ln'l'$ resonances that can contribute to ionization via the REDA channel. Reed and Chen calculated that these REDA channels are suppressed by about a factor 3 because of the loss channels described by Eq. (9). With this argument, the resonant contributions from $1s2s2ln'l'$ configurations calculated by the unified *R*-matrix theory with $n' \geqslant 5$ were reduced by a factor 3. The resulting cross sections and the conclusions that can be drawn from the comparison of these separate calculations with the experiment will be discussed below in Sec. IV.

IV. RESULTS

The present normalized scan measurement is already included in Fig. 2. Previous experimental data which are also shown in that overview picture have been discussed in the Introduction. The present *R*-matrix technique was used to determine the DI contribution to the total cross section. The result is the smooth solid line in Fig. 2. It compares very well with the other two most advanced theoretical approaches by Bray [27] and Younger [28] for DI, which are both shown in the same figure. It is interesting to note that the cross section increase beyond the EA threshold due to indirect ionization channels is not much higher than the quoted total experimental uncertainties of all the absolute cross section measurements.

Figure 4 gives an overview of the present scan measurement along with the data of Rinn *et al.* [23] to which the scan was normalized. Close inspection of the two data sets reveals small differences in the shape at the thresholds near 560 eV. Almost all of these differences would be removed by shifting the energy scale of the measurement of Rinn *et al.* downward by 2 eV, a correction that would be within the quoted uncertainty of 2.5 eV of that experiment. Remaining small differences are easily explained by a slightly higher energy spread in the ORNL data as compared to the present scan measurement. Some of the features seen in the scan measurement are assigned to specific intermediate states. Ranges of energies for configurations of the most important intermediate states are indicated (compare Fig. 1). Below the $1s2s^{2\,2}S^e$ excitation threshold only READI processes can

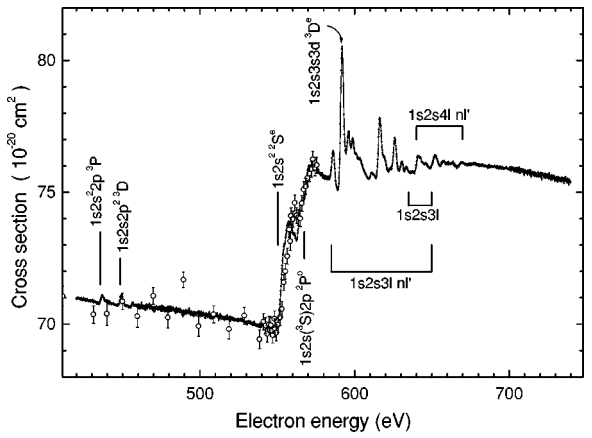

FIG. 4. Overview of the present experimental energy scan data for ionization of O^{5+} ions. The high-resolution, high-precision scan measurement is relative in nature and has to be put on an absolute scale by normalization to an absolute cross section measurement. In this work we chose to normalize the scan data to the measurement of Rinn *et al.* [23] which is represented by open circles with statistical error bars. The equivalent error bars on the present scan data are not visible on the scale of this figure. A number of levels and energy ranges of intermediate configurations are indicated.

produce resonances. At higher energies different EA channels and two series of REDA Rydberg states provide the dominant indirect ionization contributions.

Calculated ionization cross sections of O^{5+} ions are shown in Fig. 5. Bray's CCC calculation for DI [27] (dashed line), which gives results only for direct ejection of a 2s electron, is compared with the present *R*-matrix total ionization cross section, which includes DI, EA, REDA, and

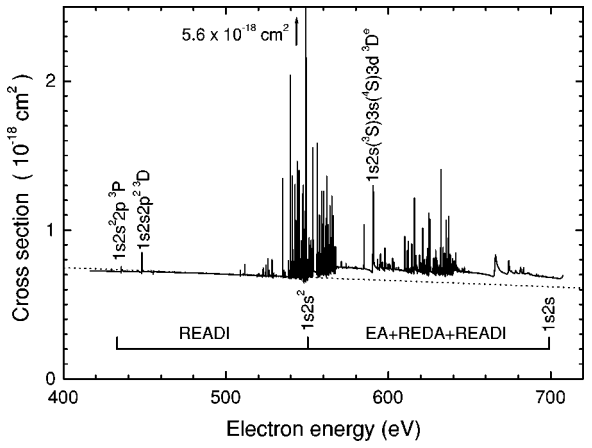

FIG. 5. Calculated electron-impact ionization cross sections for O^{5+} ions. The solid curve is the present *R*-matrix total ionization cross section with natural linewidths; the dashed line shows Bray's CCC result for DI [27]. Level assignments of several isolated resonances are provided. The READI resonance at about 548 eV reaches up to a maximum of 5.6×10^{-18} cm^2. The lowest EA threshold (at the energy of the $1s2s^2\,{}^2S$ autoionizing state) and the *K*-shell ionization threshold (at the energy of the $1s2s\,{}^3S$ state) are indicated, enclosing the range of possible REDA contributions. In addition to DI, only READI processes can contribute below the $1s2s^2$ excitation energy [cf. Eqs. (1)–(4)].

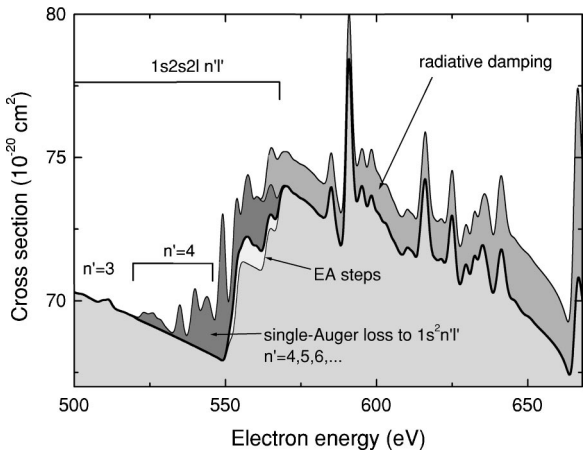

FIG. 6. Corrections applied to the present *R*-matrix total ionization cross sections. The original theoretical data from Fig. 5 have been convoluted with a 2.5 eV FWHM Gaussian to mimic the present experimental energy spread. The result is given by the uppermost curve. From this the radiation damping correction (upper shaded area as indicated, see text) has to be subtracted. The single Auger loss due to processes described by Eq. (9) indicated by the dark shaded area is subtracted according to the discussion at the end of Sec. III. The fat solid line represents the corrected theoretical cross section considered to be the best representation of electron-impact single ionization of O^{5+} ions. For comparison, the pure EA steps in the energy range 550 eV to 570 eV are also shown; these were obtained by artificially removing all resonance contributions from the total radiation-damped cross section in this energy range.

READI processes. The agreement of both calculations is excellent in the range where indirect ionization contributions are small, i.e., below 550 eV. The cross section contributions exceeding the DI calculation are the fingerprints of indirect processes. One can clearly see the contributions arising from the different ionization mechanisms: on top of the smooth DI curve are the contributions from the indirect EA, REDA, and READI processes; the resonances solely due to READI are on the left of the $1s2s^2$ EA threshold (at energies below 550.48 eV) where the REDA process is energetically forbidden; and the resonances due to both READI and REDA processes are on the right of the EA threshold (at energies above 550.48 eV). The nonresonant EA contribution approaches 10% of the total cross section. Some of the resonances in this calculation reach almost 10 times the DI cross section at their maximum. However, their contribution in a realistic experimental scenario depends on their resonance strength *S*, i.e., the area under the resonance curve. This strength becomes visible when the original *R*-matrix results are convoluted with an electron energy distribution function that resembles the experimental energy spread. (This distribution would be a Maxwellian function in the case of a plasma in thermal equilibrium.) The present experimental energy spread can be best approximated by a 2.5 eV full width at half maximum (FWHM) Gaussian. For all subsequent comparisons, the present *R*-matrix results are therefore convoluted with this experimental electron energy distribution function.

Figure 6 shows convoluted theoretical cross section contributions and corrections. The uppermost curve is obtained

TABLE II. Positions (eV) and widths (eV) of some READI resonances in O^{5+} ions. The theoretical resonance positions and widths are determined with the method [44] of Quigley and Berrington.

Resonance	Present theory Position	Present theory Width	Hofmann *et al.* Position	Bruch *et al.* Position
$1s2s^2 2p\ ^3P^o$	435.52	0.090	436.0±0.8[a]	435.9±0.2[b]
$1s2s^2 2p\ ^1P^o$	440.52	0.066		440.5±0.2[b]
$1s2s2p^2\ ^3D^e$	448.31	0.068	448.3±0.8[a]	448.5±1[c]
$1s2s2p^2\ ^3S^e$	453.87	0.033		454±1[c]
$1s2s2p^2\ ^1D^e$	455.29	0.122		457±2[c]

[a]Reference [4].
[b]Reference [45].
[c]Reference [46].

from the original *R*-matrix data displayed in Fig. 5. As described in Sec. III, radiative damping of this cross section is approximated by a reduction factor determined from the branching ratio of all the autoionization channels involving the Li-like states included in the present theory. The resulting reduction of the cross section is indicated by the upper shaded area marked ''radiative damping.''

Next, all resonances in the energy range 520 eV to 570 eV were removed from the resulting total theoretical cross section in order to investigate the influence of these resonances on the EA threshold region. The innermost shaded area results and the dominant EA steps can be clearly seen now as indicated in the figure. According to the discussion of the single Auger loss channel at the end of Sec. III, and comparing with the experimental measurement (see Fig. 4), we are convinced that indeed most of the resonance strength has to be removed from the present total *R*-matrix cross section in the energy range where $1s2s2ln'l'$ intermediate states with $n' \geqslant 4$ occur.

In the present theory, READI resonances can be identified as the resonant contributions associated with the excitation of the ground state into the pseudostates situated in the single-ionization continuum of the Li-like ion. All READI resonances in the above range are removed from the original calculation with the argument that the $1s2s2ln'l'$ intermediate states with $n' \geqslant 4$ most likely decay to singly excited (bound) states of the Li-like system and are therefore lost for the ionization channel.

The REDA contributions in the present *R*-matrix approach can be identified by their attachment to one of the doubly excited Li-like states included in the *R*-matrix basis set. Following the findings of Reed and Chen [20] we reduced the calculated contribution of REDA resonances associated with $1s2s2l$ autoionizing states by a factor 3. The resulting fat solid curve in Fig. 6 thus constitutes our best approximation of the total single-ionization cross section of O^{5+}.

In all the following figures, indirect cross section contributions rather than total cross sections are displayed. These indirect contributions are obtained by subtracting the smooth direct-ionization ''background'' from the measured and the theoretical total cross sections. In the experiment, there is some arbitrariness in this procedure since DI is not measured separately. It is clear, however, that below the EA threshold the total experimental cross section is almost solely determined by DI. The smooth cross section energy dependence observed in the range 420 eV to 550 eV can thus be extrapolated toward higher energies to obtain the DI contribution separately. The quadratic function $\sigma_{DI}=(6.856\times10^{-19}+1.648\times10^{-22}\,E-2.568\times10^{-25}\,E^2)$ cm^2 fits the experimental data of Rinn *et al.* in the energy range 400 to 550 eV. This function is subtracted from the experimental scan data to yield the cross section difference $\Delta\sigma$, i.e., the indirect ionization contributions (apart from excursions due to interference between direct and indirect ionization channels). This procedure involves quite an uncertainty resulting from the extrapolation of the DI cross section. However, it allows for the most sensitive comparison of details in theory and experiment and has been used therefore in several previous studies of indirect cross section contributions (see, e.g., [41]). The high precision of the present scan measurement with respect to cross section changes in narrow energy ranges is not influenced by this procedure but rather made to be more clearly visible. In presenting the theory, subtraction of the DI contribution is also associated with some uncertainty because a nonunified treatment is necessary to obtain the DI cross section. This results in an overall uncertainty of the size of the theoretical indirect contribution. However, the fine details occurring in narrow energy ranges that are to be compared in theory and experiment are not really influenced and can be compared best when using subtracted cross sections.

Figure 7 shows a comparison of the present experimental and corrected theoretical data in their common energy range. The agreement is very good at energies up to about 640 eV. Above that energy, the theoretical cross section drops below the experiment. We note that above 650 eV the comparison with experiment is meaningless because the highest inner-shell excitation state included in the present *R*-matrix calculation has an energy of 650.28 eV. From the several individual intermediate autoionizing states indicated in Fig. 7 one can see that the theoretical approximation, which neglects Li-like Rydberg states with quantum numbers $n \geqslant 4$, begins to break down when excitations of such states begin to come into play. In particular, the threshold energies of $1s2s3l$ excited states are around 635 eV, where the *R*-matrix calculation still produces a substantial peak feature in the cross section. Above that energy, however, Be-like $1s2s4ln'l'$ resonances ($n' \geqslant 4$) associated with $1s2s4l$ Li-like autoionizing states can occur but are not included in the present *R*-matrix calculation. Apparently, the present *R*-matrix basis set is not sufficient to account for the experimental features at energies beyond about 640 eV.

In the following four figures the details of the experimental data in comparison with theory are closely inspected. As expected from previous work [23,4] one can see four distinct EA steps in the experimental scan data of Fig. 8. These step features are associated with autoionizing states with $1s2s2l$ configurations. The states were identified in the *R*-matrix approach to be $1s2s^2\ ^2S^e$ at 550.44 eV, $1s2s(^3S)2p\ ^4P^o$ at 553.60 eV, $1s2s(^1S)2p\ ^2P^o$ at 563.26 eV, and

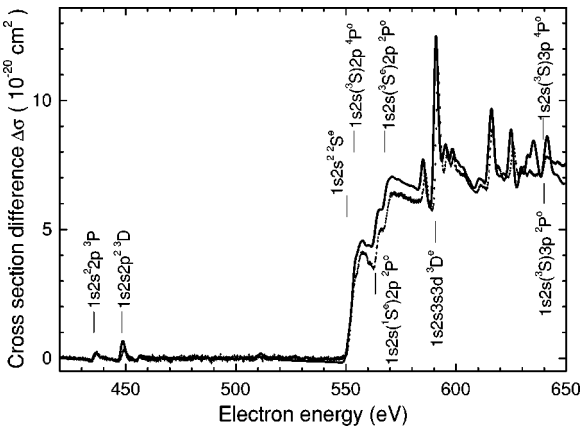

FIG. 7. Cross section contributions of indirect processes in electron-impact ionization of O^{5+} ions near the EA threshold. The data were obtained by subtracting a smooth extrapolated ''background'' of direct ionization (dominating the cross section below 550 eV) from the normalized experimental scan data displayed in Fig. 4. Some of the features in the cross section, such as excitation thresholds of specific autoionizing states including the strongest resonance ($1s2s3s3d\,^3D^e$ at a calculated energy of 590.62 eV) occurring in the measured spectrum at about 591 eV, are identified and associated with intermediate states populated during the collision. The little vertical bars shown along with the state assignments indicate the energies resulting from the present theory (cf. Tables I and II). The solid line is the cross section contribution obtained by subtracting the separately calculated *R*-matrix DI cross section from the corrected cross section displayed in Fig. 6.

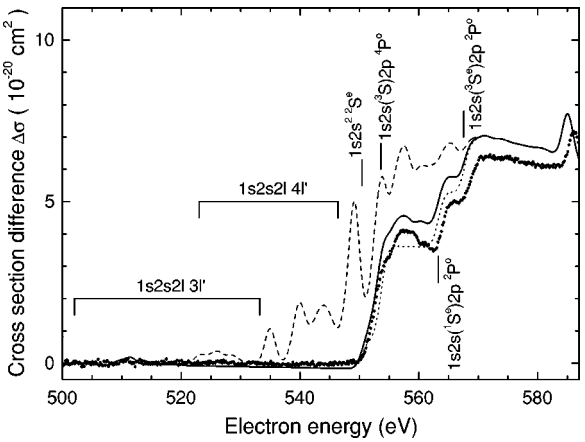

FIG. 8. Threshold region of the most important EA channels contributing to the ionization cross section of O^{5+}. The experimental scan data (solid dots with narrow spacings) and the corrected theoretical cross section curve (solid line) are the same as in Fig. 7. The dashed line shows the theoretical cross section before the subtraction of loss-channel corrections and the dotted line results when all resonance contributions between 520 eV and 570 eV are removed from the theoretical cross section. The calculated energies of the most important doubly excited states are indicated by vertical bars. The brackets indicate ranges of READI resonance positions.

$1s2s(^3)2p\,^2P^o$ at 567.58 eV. These energies are in very close agreement with the onsets of the step features in the scan data. Considering the energy spread in the measurements it becomes apparent, however, that the experimental energy scale is slightly shifted to higher energies with respect to the theory. This shift is about 1 eV, which is within the experimental uncertainty of the energy calibration.

The comparison in Fig. 8 shows that there is at most a small contribution of resonances on top of the pure EA steps in the cross section. Only around 560 eV are noticeable peak features visible. The energy dependence of these peak features is perfectly reproduced by the corrected theoretical curve. The procedure used to obtain this theoretical curve, however, is not very satisfying and more work will have to be invested in the treatment of the loss channels within the *R*-matrix formalism. Comparison of the original *R*-matrix result with the experiment clearly shows that the READI and REDA contributions associated with $1s2s2ln'l'$ states ($n' \geqslant 4$) are strongly overestimated without proper account of the loss channels.

A closer look at the measurement above the EA threshold region is taken in Fig. 9. The indirect ionization contribution from Fig. 7 is displayed in the energy range 570–630 eV. Corrections of the theoretical cross section other than for radiative damping have not been made in this energy range. The maximum indirect contribution to the total cross section stems from a REDA resonance on top of EA contributions at about 591 eV and reaches almost 15% of the total cross section at that energy. The present *R*-matrix theory gives a resonance energy of 590.62 eV for this isolated REDA resonance, which is identified to be due to the intermediate $1s2s(^3S)3s(^4S)3d\,^3D^e$ state with a natural linewidth of 0.1245 eV. The dip in the cross section just below that resonance energy indicates the presence of strong destructive interference between this very resonance and the EA channel. Clearly, the minimum at 588 eV is below the level of the EA contribution extrapolated from the flat cross section dependence in the energy range 570–583 eV. The argument for interference is supported by the fact that Reed and Chen [20], with their independent-process approximation, did not reproduce this dip feature. Tayal and Henry [19], who al-

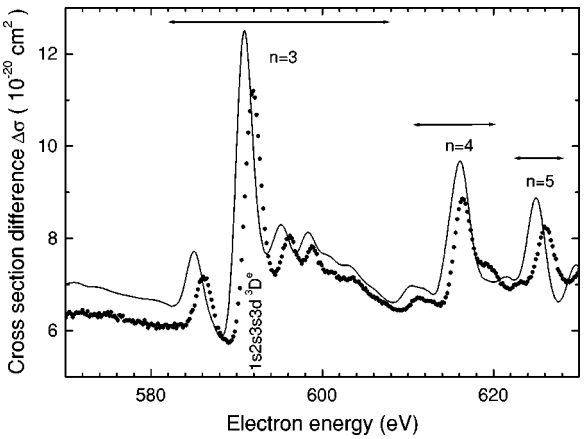

FIG. 9. Detail of Fig. 7 in the range of $1s2s3lnl'$ REDA resonances. The Rydberg groups with $n=3$, $n=4$, and $n=5$ are indicated by horizontal double arrows. The most prominent feature in the spectrum is identified as a $1s2s3s3d\,^3D^e$ resonance interfering with EA channels. The resonance energy is calculated to be 590.62 eV.

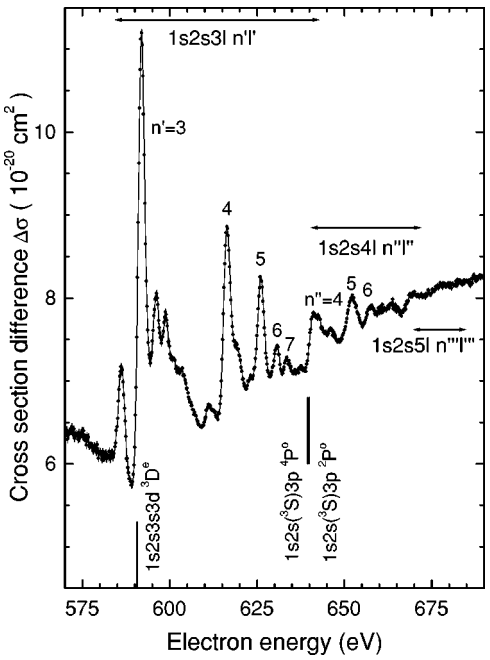

FIG. 10. Close-up of the experimental scan data in the energy range covering REDA resonances associated with $\Delta n=2$, 3, and 4 core transitions in the target ion. Resonant excitation results in the population of $1s2snln'l'$ Rydberg states with $n=3$, 4, and 5. Partially resolved fine strucure is visible within the Rydberg manifolds of the second active electron. The first series, with $n=3$, of such Rydberg states, which can still be clearly seen, ranges from principal quantum numbers $n'=3$ to $n'=7$, and the second series, with $n=4$, ranges from principal quantum numbers 4 to 6. In the third series, with $n=5$, individual Rydberg levels can hardly be distinguished, although there is still structure in the cross section visible above the $1s2s4l$ excitation threshold. The theoretical approach is known to break down in the upper half of this energy range and was left out in order to keep the fine experimental details visible. Few calculated levels are indicated.

lowed for interference between REDA and EA in their close-coupling calculation, obtained a result similar to the present calculations, which are in turn in excellent agreement with the scan experiment. At the present level of precision, fine structure within the $1s2s3l3l'$ and $1s2s3l4l'$ manifolds can be resolved. The contribution of the $1s2s3l5l'$ REDA resonances is also clearly visible. All the features in the experimental cross section arising mainly from a Rydberg series of $1s2s3lnl'$ ($n=3,4,5$) REDA resonances are perfectly reproduced by the present theory. As noted above, the experimental energy axis is slightly shifted to a higher energy. This offset is within the uncertainty of the experimental energy calibration.

Figure 10 displays an overview of the experimental details found beyond 570 eV. It is obvious from Fig. 7 that the present *R*-matrix approach breaks down at energies beyond about 640 eV. Therefore, the theory curve is not shown here again. The dominating REDA resonance identified as $1s2s3s3d\,^3D^e$ at 590.62 eV belongs to a series of Rydberg levels with configurations $1s2s3ln'l'$ where $n'\geqslant 3$. As mentioned above, the $n'=3$ fine structure is partly resolved and the whole resonance group associated with configura-

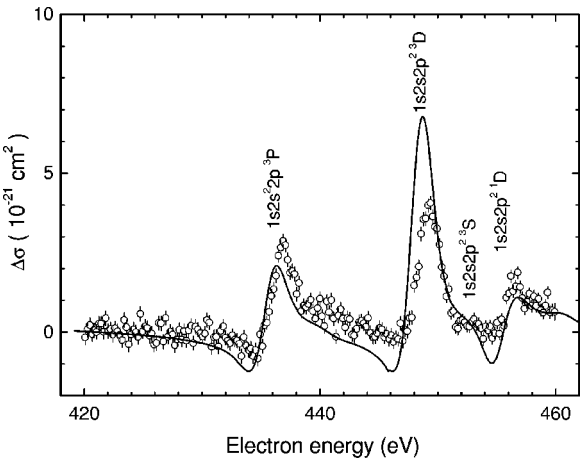

FIG. 11. Comparison of theory and experiment in the range of dominant READI contributions. The data are the same as in Fig. 7, just enlarged for detailed inspection. The READI resonances in this energy range are identified and associated with the related cross section features.

tions $1s2s3l3l'$ covers an energy range of about 30 eV. Also, the next member of the $1s2s3ln'l'$ Rydberg series with $n'=4$ shows partially resolved fine structure, and configurations with $n'=5$, 6, and even 7 can be clearly distinguished in the experimental data. The series limits of these Rydberg resonances ($n'\rightarrow\infty$) are associated with doubly excited Li-like states with configurations $1s2s3l$. The level energies of two of the states [$1s2s(^3S)3p\,^4P^o$ and $1s2s(^3S)3p\,^2P^o$] associated with such configurations are taken from the present *R*-matrix calculation and indicated in the figure. Excitation of autoionizing $1s2s3l$ states at energies above approximately 640 eV produces a distinct step feature in the experimental cross section. Resonances above the $1s2s3l$ EA thresholds have to be associated with Be-like $1s2s4ln''l''$ states. Again, the REDA group with the lowest principal quantum number $1s2s4l4l''$ appears to be partly resolved while the $n''=5$ and $n''=6$ Rydberg states just produce single-peak features in the experimental scan. From the step feature observed at about 568 eV, one might conclude that $1s2s4l$ EA contributions are present. Above that energy, one has to expect REDA associated with $1s2s5ln'''l'''$ with $n'''\geqslant 5$. Although the cross section still shows peak structures in that range, a real identification of such double Rydberg states is not possible on the basis of the present experiment.

The final comparison of the present experiment with the *R*-matrix calculations deals with the energy range 420–460 eV where READI is important. The results are provided in Fig. 11. As already mentioned in connection with Fig. 9, the theory curve was not manipulated in this energy range by subtracting heuristic contributions. Instead, the figure shows the original results of the present READI calculation, enlarged from Fig. 7. The cross section difference $\Delta\sigma=\sigma(E)-\sigma_{DI}$ representing the experimental contribution of indirect ionization mechanisms is slightly altered as compared to Fig. 7. Although the simple quadratic function employed so far to represent the experimental direct ionization contribution σ_{DI} coincides well with the measurement of Rinn *et al.*, it is not

totally adequate for representing the present scan measurement $\sigma(E)$ when it comes to a comparison at the level of 10^{-21} cm^2, i.e., when looking at differences of the order of 0.15% of the total cross section. A better representation of the direct ionization contribution in the limited energy range from 420 eV to 460 eV is given by $\sigma_{DI}=(7.7842\times10^{-19}-1.5873\times10^{-22}E)$ cm^2. This deviates from the overall fit given above by only $+2\times10^{-21}$ cm^2 at 420 eV and -1.5×10^{-21} cm^2 at 460 eV which is a tiny difference in the total cross section but makes a real difference in the interpretation of the READI features. Therefore this slightly different background was subtracted from the experimental data points just in the limited energy range covered by Fig. 11. This additional subtraction was necessary in order to provide a meaningful indirect-ionization cross section $\Delta\sigma$ in that energy range for comparison with the theory. The resulting experimental data exhibit an excursion to slightly negative values at around 435 eV indicating the presence of interference between READI and DI. The theoretical curve shows such destructive interference patterns even more strongly and suggests that even a slightly higher DI ''background'' might have to be subtracted from the experimental data. The experiment itself, however, does not provide immediate justification of this extra manipulation. We note that we have tried here to represent the DI cross section in different energy ranges of interest by the simplest possible function. Constructing a universal smooth function representing the DI cross section at all energies would certainly be possible but would require a multiparameter fit of a complicated but smooth function to the experimental data. Such an effort does not seem to be justified considering the uncertainty of the DI cross section σ_{DI} in both theory and experiment.

With this in mind, Fig. 11 shows a very satisfying agreement of theory and experiment, which strongly supports the interpretation of destructive interference of a complex resonant ionization channel with the dominating direct ionization process. It is remarkable that such a feature can be seen in the total ionization cross section. Interference patterns are usually seen much more strongly in angular differential cross section studies.

As in a previous study [13] on the ionization of C^{3+} ions by electron impact, we find that the $1s2s^22p\,^3P^o$ READI resonance (at 435.52 eV in the case of O^{5+}) with its asymmetric shape is reproduced extremely well by the *R*-matrix calculation, while the second prominent $1s2s2p^2\,^3D^e$ READI resonance (found at 448.31 eV) is substantially overestimated by the theory. While both these features have been observed previously, with much larger error bars, the smaller features at 453 eV and 457 eV have not, to our knowledge. According to the present *R*-matrix approach they are associated with $1s2s2p^2\,^3S^e$ (at 453.87 eV) and $1s2s2p^2\,^1D^e$ (at 455.29 eV) states.

Following the arguments discussed at the end of Sec. III, the READI resonances displayed in Fig. 11 are also subject to the influence of different loss channels. For example, the $1s2s^22p\,^3P$ state can undergo a single Auger decay to a bound $1s^22l$ state, the decay rate of which has been calculated by Pindzola and Griffin to be $P_s=1.42\times10^{14}$ s^{-1} [18]. Chen and Crasemann [42] found a value 1.29×10^{14} s^{-1}. This loss channel is accounted for in the present *R*-matrix calculation by the inclusion of all $1s^22s$ and $1s^22p$ basis states. The double Auger rate is included in the present calculation by the resonant contributions to the excitation of the continuum pseudostates that represent the READI mechanism. Clearly, the decay probability P_d for double Auger decay is very much smaller (between $P_d=1.5\times10^{11}$ s^{-1} and $P_d=1.15\times10^{12}$ s^{-1} [18]) than that of the single Auger decay. The loss channel not considered in the present calculation is radiative stabilization: $1s2s^22p\,^3P\rightarrow1s^22s2l+h\nu$. The probability for this decay is $P_r=8.34\times10^{10}$ s^{-1} [42]. This means that the present ionization amplitude for the $1s2s^22p\,^3P$ READI resonance in principle should be corrected by a factor $(P_d+P_s)/(P_d+P_s+P_r)\approx0.9994$. This is so close to 1 that radiative corrections can be totally ignored. For the $1s2s2p^2\,^3D$ READI resonance the situation is quite similar.

The only additional correction that is not included in the present *R*-matrix calculation and that could possibly influence the dominant READI features visible in Fig. 11 is due to loss channels of the kind $1s2s2l2l'\rightarrow1s^2nl+e$ with $n\geqslant4$. If the decay rate for such shake-up processes is termed $P_s^{(n)}$, the correction factor for the present READI amplitude will be $P_s/(P_s+P_s^{(n)})$. Shake-up probabilities have not been calculated for the processes of interest here. We assume that shake-up to Rydberg states with $n\geqslant4$ has a low probability compared with regular single Auger decay to $1s^22l$ states. Hence, the expected correction for the lowest READI resonances as displayed in Fig. 11 would be small and therefore cannot explain the differences in the level of agreement between theory and experiment for the dominating READI peaks.

V. CONCLUSIONS

In conclusion, the current experimental measurement, with its high precision and energy resolution, allows us to observe much finer details in the ionization cross section than in previous studies. In particular, really quantitative data have become accessible for the strongest READI resonances occurring at the lowest energies where indirect processes can contribute to the ionization cross section. In this way, the observation of interference between DI and READI in a previous study on the ionization of C^{3+} [13] has now been confirmed for O^{5+} also.

The precision of the present experimental data facilitates a very critical test of the unified *R*-matrix approach and its capability to handle fine details in the ionization cross section as a result of indirect ionization mechanisms. While many cross section features arising from the EA, REDA, and READI processes are very well reproduced by the calculations, the comparison also reveals some of the weaknesses of the present unified *R*-matrix approach with its limited basis set for the construction of the total wave function. In future work the effect of the single Auger loss channels should be treated in the unified *R*-matrix calculation on more solid grounds compared to the heuristic approach used in this study. For higher ion charge states it will also be necessary to find a more elaborate treatment of radiative damping of

autoionizing states, while retaining the advantages of the unified *R*-matrix approach.

ACKNOWLEDGMENTS

We would like to thank Professor P. G. Burke for providing us with a copy of the RMATRX II package, and Dr. S. Schippers and Dr. N. R. Badnell for useful discussions. Support of the present work by Deutsche Forschungsgemeinschaft, Bonn, is very gratefully acknowledged. Participation of one of us (R.A.P.) in the experiments was made possible by a NATO collaborative research grant.

[1] A. Müller, in *Physics of Ion Impact Phenomena*, Vol. 54 of *Springer Series in Chemical Physics*, edited by D. Mathur (Springer-Verlag, Berlin, 1991), pp. 13–90.
[2] D. L. Moores and K. J. Reed, Adv. At., Mol., Opt. Phys. **34**, 301 (1994).
[3] A. Müller, G. Hofmann, K. Tinschert, and E. Salzborn, Phys. Rev. Lett. **61**, 1352 (1988).
[4] G. Hofmann, A. Müller, K. Tinschert, and E. Salzborn, Z. Phys. D: At., Mol. Clusters **16**, 113 (1990).
[5] A. Müller, G. Hofmann, K. Tinschert, B. Weißbecker, and E. Salzborn, Z. Phys. D: At., Mol. Clusters **15**, 145 (1990).
[6] B. Peart, J. W. G. Thomason, and K. Dolder, J. Phys. B **24**, 4453 (1991); **24**, 489 (1991).
[7] J. Kenntner, J. Linkemann, N. R. Badnell, C. Broude, D. Habs, G. Hofmann, A. Müller, M. S. Pindzola, E. Salzborn, D. Schwalm, and A. Wolf, Nucl. Instrum. Methods Phys. Res. B **98**, 142 (1995).
[8] J. Linkemann, J. Kenntner, A. Müller, A. Wolf, D. Habs, D. Schwalm, W. Spies, O. Uwira, A. Frank, A. Liedtke, G. Hofmann, E. Salzborn, N. R. Badnell, and M. S. Pindzola, Nucl. Instrum. Methods Phys. Res. B **98**, 154 (1995).
[9] J. Linkemann, A. Müller, J. Kenntner, D. Habs, D. Schwalm, A. Wolf, N. R. Badnell, and M. S. Pindzola, Phys. Rev. Lett. **74**, 4173 (1995).
[10] T. W. G. Thomason and B. Peart, J. Phys. B **31**, 210 (1998).
[11] K. A. Berrington, J. Pelan, and L. Quigley, J. Phys. B **30**, 4973 (1997).
[12] M. P. Scott, H. Teng, and P. G. Burke, J. Phys. B **33**, L63 (2000).
[13] H. Teng, H. Knopp, S. Ricz, S. Schippers, K. A. Berrington, and A. Müller, Phys. Rev. A **61**, 060 704(R) (2000).
[14] Z. Felfi, K. A. Berrington, and A. Z. Msezane, J. Phys. B **33**, 1263 (2000).
[15] H. Teng, J. Phys. B **33**, L553 (2000).
[16] K. Berrington and S. Nakazaki, J. Phys. B **31**, 313 (1998).
[17] H. Teng, J. Phys. B **33**, L227 (2000).
[18] M. S. Pindzola and D. C. Griffin, Phys. Rev. A **36**, 2628 (1987).
[19] S. S. Tayal and R. J. W. Henry, Phys. Rev. A **44**, 2955 (1991).
[20] K. J. Reed and M. H. Chen, Phys. Rev. A **45**, 4519 (1992).
[21] D. H. Crandall, R. A. Phaneuf, B. E. Hasselquist, and D. C. Gregory, J. Phys. B **12**, L249 (1979).
[22] D. H. Crandall, R. A. Phaneuf, D. C. Gregory, A. M. Howald, D. W. Mueller, T. J. Morgan, G. H. Dunn, D. C. Griffin, and R. J. W. Henry, Phys. Rev. A **34**, 1757 (1986).
[23] K. Rinn, D. C. Gregory, L. J. Wang, R. A. Phaneuf, and A. Müller, Phys. Rev. A **36**, 595 (1987).
[24] A. Müller, K. Tinschert, G. Hofmann, E. Salzborn, and G. H. Dunn, Phys. Rev. Lett. **61**, 70 (1988).
[25] N. R. Badnell, M. S. Pindzola, I. Bray, and D. C. Griffin, J. Phys. B **31**, 911 (1998).
[26] D. M. Mitnik, M. S. Pindzola, D. C. Griffin, and N. R. Badnell, J. Phys. B **32**, L479 (1999).
[27] I. Bray, J. Phys. B **28**, L247 (1995).
[28] S. M. Younger, J. Quant. Spectrosc. Radiat. Transf. **26**, 329 (1981).
[29] K. Tinschert, A. Müller, G. Hofmann, K. Huber, R. Becker, D. C. Gregory, and E. Salzborn, J. Phys. B **22**, 531 (1989).
[30] M. Liehr, M. Schlapp, R. Trassl, G. Hofmann, M. Stenke, R. Völpel, and E. Salzborn, Nucl. Instrum. Methods Phys. Res. B **79**, 697 (1993).
[31] A. Müller, K. Huber, K. Tinschert, R. Becker, and E. Salzborn, J. Phys. B **18**, 2993 (1985).
[32] R. Becker, A. Müller, Ch. Achenbach, K. Tinschert, and E. Salzborn, Nucl. Instrum. Methods Phys. Res. B **9**, 385 (1985).
[33] K. Rinn, A. Müller, H. Eichenauer, and E. Salzborn, Rev. Sci. Instrum. **53**, 829 (1982).
[34] H. A. Yamani and W. P. Reinhard, Phys. Rev. A **11**, 1144 (1975).
[35] A. W. Weiss, Astrophys. J. **138**, 1262 (1963).
[36] A. Hibbert, Comput. Phys. Commun. **9**, 141 (1975).
[37] P. G. Burke, V. M. Burke, and K. M. Dunseath, J. Phys. B **27**, 5341 (1994).
[38] M. J. Seaton, J. Phys. B **18**, 2111 (1985).
[39] NIST Atomic Spectra Database web site: http://physics.nist.gov/cgi-bin/AtData/levels_form
[40] F. Robicheaux, T. W. Gorczyca, M. S. Pindzola, and N. R. Badnell, Phys. Rev. A **52**, 1319 (1995).
[41] A. Müller, G. Hofmann, B. Weißbecker, M. Stenke, K. Tinschert, M. Wagner, and E. Salzborn, Phys. Rev. Lett. **63**, 758 (1989).
[42] M. H. Chen and B. Crasemann, At. Data Nucl. Data Tables **37**, 419 (1987).
[43] M. Rødbro, R. Bruch, and P. Bisgaard, J. Phys. B **12**, 2413 (1979).
[44] L. Quigley and K. A. Berrington, J. Phys. B **29**, 4529 (1996).
[45] R. Bruch, S. Datz, P. D. Miller, P. L. Pepmiller, H. F. Krause, J. K. Swenson, and N. Stolterfoht, Phys. Rev. A **36**, 394 (1987).
[46] R. Bruch, D. Schneider, W. H. E. Schwarz, M. Meinhart, K. Taulbjerg, and B. M. Johnson, Phys. Rev. A **19**, 587 (1979).